OPEN ACCESS

Planetary Sciences ARTICLE

The Innovation Geoscience

Soluble organic matter evolution during aqueous alteration in carbonaceous chondrites

Mingtan Dong,[1,2] Wei Yang,[1,*] Jialong Hao,[1] Sen Hu,[1] and Yangting Lin[1]

*Correspondence: yangw@mail.iggcas.ac.cn

Received: November 12, 2025; Accepted: January 26, 2026; Published Online: January 28, 2026; https://doi.org/10.59717/j.xinn-geo.2026.100199

GRAPHICAL ABSTRACT

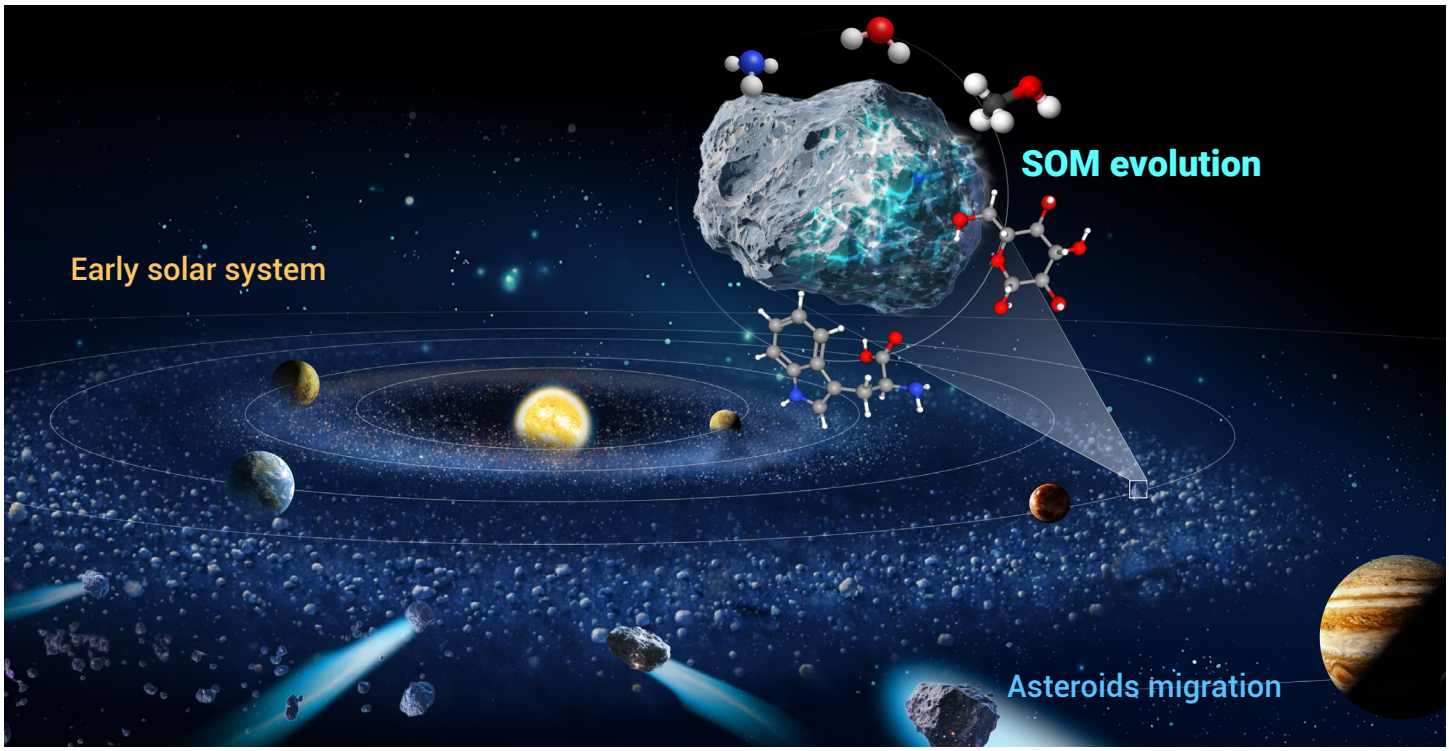

PUBLIC SUMMARY

- We analyzed the composition, abundance and distribution of soluble organic matter (SOM) in meteorites.
- Desorption electrospray ionization mass spectrometry imaging mapped SOM at ~10 μm resolution.
- SOM is distributed in phyllosilicates and concentrated in fine-grained rims of chondrules.
- Parent-body source and aqueous alteration jointly shape SOM synthesis and preservation.

ARTICLE Planetary Sciences

www.the-innovation.org/geoscience

Soluble organic matter evolution during aqueous alteration in carbonaceous chondrites

Mingtan Dong,[1,2] Wei Yang,[1,*] Jialong Hao,[1] Sen Hu,[1] and Yangting Lin[1]

[1]Key Laboratory of Earth and Planetary Physics, Institute of Geology and Geophysics, Chinese Academy of Sciences, Beijing 100029, China

[2]University of Chinese Academy of Sciences, Beijing 100049, China

*Correspondence: yangw@mail.iggcas.ac.cn

Received: November 12, 2025; Accepted: January 26, 2026; Published Online: January 28, 2026; https://doi.org/10.59717/j.xinn-geo.2026.100199

Citation: Dong M., Yang W., Hao J., et al. (2026). Soluble organic matter evolution during aqueous alteration in carbonaceous chondrites. *The Innovation Geoscience* **4**:100199.

Soluble organic matter (SOM) in meteorites has been suggested to play a significant role in the emergence of early life on Earth. However, the mechanisms that govern its evolution remain unclear. Here, we employed an integrated analytical approach encompassing desorption electrospray ionization high-resolution mass spectrometry (DESI-HRMS) imaging and ultra-high-performance liquid chromatography–high-resolution mass spectrometry (UHPLC-HRMS) to comprehensively analyze the composition, abundance, and spatial distribution of methanol-extractable SOM in nine meteorites with different alteration histories. The results show that SOM is preferentially associated with phyllosilicates but depleted in carbonate phases. A positive correlation is observed between the abundance of SOM and the degree of aqueous alteration in CM2 chondrites, although highly altered CI1 chondrites deviate from this trend. Additionally, the composition of SOM appears to be modulated by fluid redox conditions and heliocentric distance, as indicated by systematic differences in molecular features among chondrites from different parent bodies. The findings suggest that the evolution of SOM is governed by the coupled influences of the Solar System environment, parent-body processes, and microscale mineral phases, with aqueous alteration and fluid activity serving as the central driving forces.

INTRODUCTION

Organic matter has been detected in a variety of carbonaceous chondrites[1,2] and in extraterrestrial samples returned from carbonaceous chondrite-like asteroids Ryugu and Bennu.[3-5] The delivery of extraterrestrial organic matter to Earth via meteorites has been proposed as a potential contributor to the building blocks of life.[6,7] Organic matter in meteorites is commonly divided into solvent soluble organic matter (SOM)[3] and solvent/acid insoluble organic matter (IOM).[5] SOM is characterized by a vast chemical diversity, comprising tens of thousands of molecules.[1,3,4] It is hypothesized that SOM may have been more readily utilized by early life, as it contains small molecules essential for life processes, including amino acids, fatty acids, nucleobases and sugars.[2,8-13] Despite its potential prebiotic significance, the mechanisms underlying the formation, evolution and preservation of SOM remain unclear because of a paucity of direct evidence.[2]

Current hypotheses suggest that the formation and evolution of SOM occur through multiple sequential stages: beginning in the interstellar medium (ISM), proceeding through the protostellar disk and planetesimal aggregation, and continuing with subsequent alteration within asteroid parent bodies.[2,14] Isotopic evidence supports this scenario, as enrichments in D and ^{15}N in meteoritic organic matter deviate markedly from Solar System average values,[3] consistent with isotope fractionation processes in the cold environments of the ISM.[2] In such environments, high-energy ultraviolet photons and cosmic rays generate abundant radicals, providing key precursors for SOM synthesis.[2,15] Laboratory simulations have demonstrated that low-temperature ultraviolet irradiation of interstellar ice analogs can produce a variety of organic compounds, including SOM-like species.[15-17] Astronomical observations also reveal that relatively simple N-, O-, and S-bearing organic molecules are widespread in the ISM,[18] where they can adsorb onto dust grains and be incorporated into growing planetesimals and asteroid parent bodies.[19] While some simple organics and amino acids may survive transit through the harsh ISM conditions,[20-23] the formation, evolution, and preservation of larger and more complex SOM species (~100–800 Da)[24] remain poorly understood.[2] Addressing this knowledge gap requires a comprehensive characterization of SOM composition, abundance, and occurrence, with particular emphasis on their spatial associations with inorganic minerals. Such an approach enables molecular signatures to be linked directly to parent-body processes, thereby constraining the mechanisms responsible for SOM formation and evolution.[25]

To achieve this, robust analytical strategies are essential. The analysis of SOM in meteorites and asteroid samples can be broadly categorized into targeted and untargeted strategies. Targeted approaches typically focus on life-relevant compounds, such as amino acids. Untargeted analysis has traditionally been dominated by direct-injection Fourier transform ion cyclotron resonance mass spectrometry (FT-ICR/MS),[3,4] which enables the assignment of tens of thousands of molecular formulas owing to its ultra-high mass resolution (> 10^7) and sub-ppm mass accuracy.[24,26] Comparative studies based on FT-ICR/MS have revealed substantial differences in SOM composition across meteorites and asteroid samples.[24,26] However, *in-situ* SOM analysis remains scarce. Desorption electrospray ionization high-resolution mass spectrometry (DESI-HRMS) imaging has been applied to meteorites and Ryugu samples,[3,25,27-30] but previous spatial resolution has not been sufficient to systematically resolve the SOM distribution among distinct mineral phases or structures. Our earlier work improved DESI spatial resolution to 20 μm,[31] and in the present study we further enhanced it to ~10 μm, thereby making it increasingly feasible to elucidate SOM–mineral associations. In parallel, ultra-high-performance liquid chromatography–high-resolution mass spectrometry (UHPLC-HRMS)[32,33] has emerged as a powerful untargeted analytical platform in metabolomics[34] and prebiotic chemistry.[35,36] Its chromatographic separation improves quantitative accuracy and enables direct comparisons of SOM across multiple samples.[37,38]

In this context, we combine DESI-HRMS imaging and UHPLC-HRMS to systematically characterize the composition, abundance, and spatial distribution of methanol-extracted SOM in nine fallen meteorites representing diverse petrographic types and degrees of aqueous alteration. This integrated approach provides new insights into the origin and evolution of SOM in extraterrestrial environments, with a particular emphasis on the role of parent-body aqueous alteration in its formation and preservation.

MATERIALS AND METHODS

Sample information

The names, classifications, and fallen year of meteorites are as follows: Zag (H3-6, 1998),[39] Allende (CV3, 1969),[40] Ningqiang (C3-ungrouped, 1983),[41] Murchison (CM2.5, 1969),[42] Aguas Zarcas (CM2.2, 2019),[43] Mukundpura (CM2.0, 2017),[44] Kolang (CM1/2, 2020),[45] Tarda (C2-ungrouped, 2020)[46,47] and Orgueil (CI1, 1864).[48,49] Their petrological and isotopic characteristics have been extensively documented, and the presence of organic matter within their matrices has been confirmed by previous studies. Compared to samples from currently available asteroid sample-return missions, fallen meteorites offer far greater sample diversity, making them an essential resource for understanding the evolution of SOM in asteroids. Although restricting our study to meteorite falls helps minimizes the potential impacts of terrestrial contamination and alteration on SOM,[50] such influences cannot be entirely excluded.

For each meteorite, one portion was used for solvent extraction of SOM, and another portion was prepared as a polished cross-section for DESI analysis. Although organic matter has been previously reported in the water-bearing salt crystals and clasts within Zag,[39,51] such components were not clearly observed in the subsample analyzed in this study (Figures S1-S2).

Meteorite cross-section sample preparation

Each meteorite sample was affixed to a stub using a minimal amount of adhesive. A smooth, large-area cross-section was then prepared using a target preparation system (Leica EM TXP) combined with a broad argon ion milling system (Leica EM TIC 3X). This method avoided the need for resin embedding, slurry polishing, and solvent cleaning. To minimize heat buildup during milling, alternating ion beam conditions were applied: samples underwent four cycles at 5 keV and 2 mA, with each cycle lasting 20 minutes, followed by three cycles at 1 keV and 1 mA, with each cycle lasting 10 minutes.[31] All cycles were conducted at an ion beam incidence angle of 3°.

DESI-HRMS imaging analysis

DESI-HRMS imaging was performed using a platform consisting of a DESI XS source (Waters), a high-resolution mass spectrometer (SELECT SERIES MRT, Waters), and a solvent delivery system (ACQUITY UPLC M-Class μBSM, Waters).[52] To facilitate comparison with earlier meteorite studies that employed DESI-HRMS in positive-ion mode,[25,27-29] imaging was conducted in positive-ion mode as well. The solvent used was a mixture of methanol and water (95:5, v/v). Samples were scanned with a step size of 10 μm, a solvent flow rate of 250 nL·min^{-1}, and a scan speed of 20 μm·s^{-1}. Detailed instrumental parameters are provided in Table S1. In comparison with our previous study on the Murchison meteorite,[31] which achieved a spatial resolution of 20 μm, a mass resolution of ~30,000 at 556 Da, and a mass accuracy of < 15 ppm, the present study achieved a higher spatial resolution of ~10 μm (Figure S3), an ultrahigh mass resolution of ~160,000 at 556 Da, and a mass accuracy of < 1 ppm.[53] Since DESI-HRMS can only ionize SOM, these technical advancements enable more precise discrimination of SOM associated with different minerals (Figures 1-3) and allow for reliable molecular formula assignment for detected compounds.

Methanol is widely used in DESI analysis,[27,28,31] providing efficient extraction and ionization of polar and moderately polar organics. Previous studies have demonstrated that methanol, compared to other solvents such as water or acetonitrile, extracts a broader range of SOM from meteorites.[1] The DESI source exhibits relatively low ionization efficiency for non-polar compounds,[54] and the combination of a methanol-water solvent and DESI ionization provides high extraction and ionization efficiency for polar SOM, thereby achieving low detection limits for these species. However, this approach is less effective for non-polar SOM, and a more comprehensive characterization of SOM would benefit from employing multiple solvent systems in future studies.

Quality assurance for DESI-HRMS imaging

Fused silica cross-section samples (Corning 7980 0F, Edmund) were prepared in parallel with the meteorite samples and served as procedure blanks to monitor potential contamination during sample preparation. Fused silica was selected due to its high thermal stability and extremely low background organic content,[4,8] as its production involves temperatures exceeding 1700°C, thereby excluding the presence of indigenous SOM. Moreover, its low surface porosity minimizes solvent retention and surface heterogeneity, contributing to enhanced DESI signal intensity and sensitivity. A glass slide was used as the solvent blank. All cross-section samples were stored and transported between laboratories in a vacuum-sealed metal container. All reagents were LC-MS grade (Fisher Chemical). No evidence of additional contamination was observed during sample preparation (Figures S4-S5). Ions detected in the solvent or procedural blanks were excluded from subsequent analysis and discussion.

Fused silica may not fully represent the physical and chemical characteristics of meteoritic surfaces. Mineralogical and structural differences—such as surface energy, porosity, and roughness—may lead to discrepancies in matrix effects and potential adsorption of exogenous contaminants. While fused silica serves as a conservative and contamination-free reference, future studies could explore mineral analogues (e.g., serpentine)[3] more representative of meteoritic matrices to better evaluate contamination risks and matrix effects.

DESI-HRMS data processing

Centroid peak features were extracted from the raw DESI-HRMS data using HDI v1.8 (Waters) and used to generate raster images for each detected m/z feature. The molecular formulas were then assigned in MassLynx v4.2 (Waters) within a mass tolerance of 1 ppm, using the peak positions exported from HDI v1.8 and applying the following elemental constraints: C 0-100, H 0-100, N 0-10, O 0-20, and S 0-2. Because only the centroid peak positions were imported, isotope peaks of low-intensity ions were not always captured. Consequently, isotope pattern fitting was not used as a criterion during formula assignment. Sulfur-bearing formulas were cross-validated against those independently obtained from the UHPLC-HRMS data. A magnified profile mass spectrum extracted from an arbitrary time window of the raw total ion chromatogram was used to illustrate peak separation, with molecular formulas and mass errors annotated manually (Figure 2B). Due to peak-shape shift and signal-to-noise limitations, some annotated mass errors in this magnified spectrum exceed 1 ppm.

Guided by the SEM–EDS results, specific mineral phases or regions of interest were selected, and location-specific average DESI-HRMS spectra were extracted for comparative and multivariate analysis, including violin plots (Figure 2C) and principal component analysis (PCA) (Figure 2D).

In DESI-HRMS analysis, ion signal intensities are influenced not only by the concentration of the analytes, but also by matrix effects arising from the physical and chemical properties of the sample substrate, such as mineral composition, surface roughness, and porosity.[55] For example, highly porous rock surfaces can reduce ion yield in DESI analysis.[55] In addition, during the ionization process, ion suppression and charge competition may occur,[54] which are related to the chemical complexity and coexisting species in the sample. Matrix effects result in signal intensities that do not necessarily reflect the actual abundance of SOM.[31] To correct for intra-sample matrix effects, the intensity of the lockmass ion (leucine enkephalin, 50 ng·ml^{-1}) added to the solvent was used to normalize all detected signals,[31,56] enabling a more accurate representation of the spatial distribution of SOM within the same sample (Figure S6).[31] However, it should be noted that this normalization only compensates for matrix effects within a given sample, and thus, direct comparison of DESI-HRMS signal intensities between different samples remains infeasible at present.

SEM-EDS analysis

After DESI-HRMS imaging, large-area backscattered electron (BSE) images (Figure S2) were acquired using a low-vacuum desktop scanning electron microscope (Phenom XL G2, Thermo Fisher Scientific) equipped with an integrated energy dispersive X-ray spectroscopy (EDS) system. The instrument was operated at 60 Pa and 15 kV, with data acquisition performed using MAPS v3.29 software (Thermo Fisher Scientific).

SOM extraction

To ensure consistency with DESI-HRMS results, methanol extraction was used to isolate SOM from powdered meteorite samples. We powdered interior fragments while avoiding fusion crusts and visibly weathered surfaces. Approximately 60 mg of meteorite fragments were ground into a fine powder, and ~10 mg of powder was weighed into individual 1.5 mL microcentrifuge tubes. Methanol was added at a ratio of 20 μL per 1 mg of sample.[3] The SOM was extracted via ultrasonication for 15 minutes. The extract was then centrifuged at 12,000 rpm for 10 minutes, and the resulting supernatant was carefully transferred into a screw-neck vial containing a low-volume insert.

UHPLC-HRMS analysis

SOM extracts in methanol were analyzed using an ACQUITY Premier UPLC system (Waters) coupled to a quadrupole Multi-Reflecting Time-of-Flight (Q-MRT) mass spectrometer (SELECT SERIES MRT, Waters) equipped with an electrospray ionization (ESI) source, providing ultra-high mass resolution (~200,000) and mass accuracy (< 1 ppm).[53] To maintain consistency with DESI-HRMS imaging, UHPLC-HRMS analysis was also conducted in ESI positive-ion mode. The mobile phase comprised acetonitrile and water, and the separations were performed using a BEH C18 column (130 Å, 1.7 μm, 2.1 mm x 100 mm, Waters). Data acquisition was performed using MS^E, a data-independent acquisition (DIA) mode that enables enhanced MS^2 spectral coverage.[57] Progenesis QI software (v3.0, Waters) was used for data analysis, including alignment, peak picking, deconvolution, and identification. Statistical analysis was carried out using EZinfo v3.0 (Waters). Detailed instrument

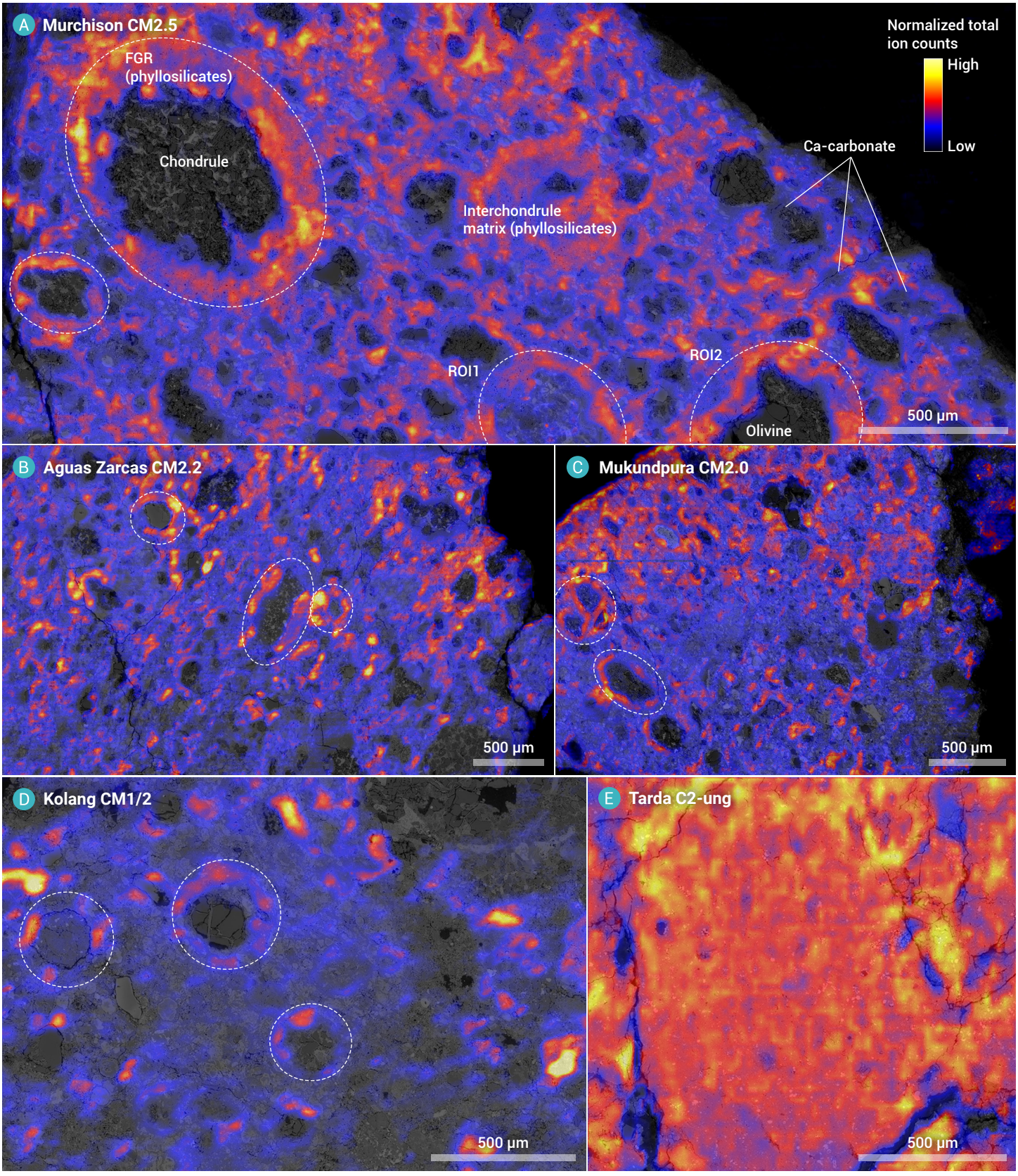

Figure 1. Spatial distribution of SOM in CM chondrites and Tarda (C2-ung) (A-E) Normalized total ion counts of SOM compounds detected by DESI-HRMS imaging, overlaid with backscattered electron images. The dashed line outlines the fine-grained rims (FGRs) surrounding chondrules. The darker areas in panel (E) represent cracks rather than chondrules. In panel (A), labels ROI1 and ROI2 mark an aqueously altered chondrule and an unaltered, primitive chondrule lacking aqueous alteration features, respectively. Note that the color bars reflect normalized total ion counts within each panel only and are not used for intensity comparisons between panels.

parameters and data processing protocols are provided in Table S2.

The inclusion of liquid chromatography not only reduces ion suppression effects but also improves the detection limits for moderately and weakly polar SOM, thus enabling more accurate quantification and between-sample comparisons of SOM abundance. The chemical coverage of SOM by UHPLC-HRMS can be further improved by adding HILIC chromatography, using

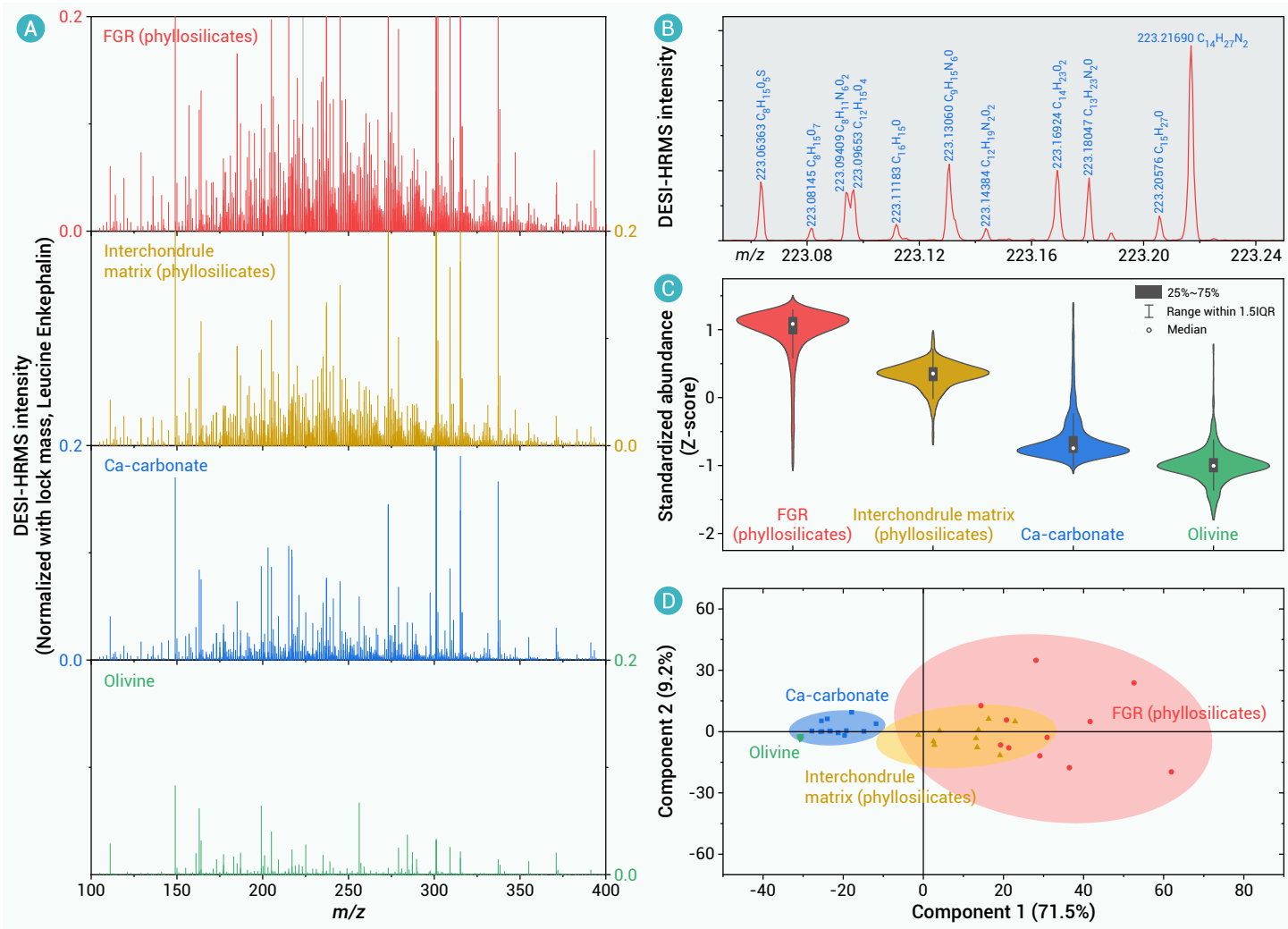

Figure 2. Mineral- and structure-specific differences in SOM within the Murchison (CM2.5) meteorite revealed by DESI-HRMS imaging (A) DESI-HRMS spectra (positive ion mode) of SOM extracted from distinct mineralogical and structural domains: phyllosilicates in fine-grained rims (FGRs), phyllosilicates in the interchondrule matrix, Ca-carbonate, and olivine. Ion signals from olivine are primarily attributed to solvent background. (B) Expanded view of the DESI-HRMS profile spectrum in the range of 223.05–223.25 Da, extracted directly from the raw total ion chromatogram. In order to create this illustrative profile spectrum, the molecular formulas were annotated manually. Consequently, some labeled m/z values deviate by more than 1 ppm from the calculated formula values. (C) Standardized abundance (Z-score) distributions of SOM in each domain. (D) Principal component analysis (PCA) of SOM across mineral domains. Ellipses represent the 95% confidence intervals.

multiple ionization sources and polarities [e.g., ESI(+/−), APCI], and employing complementary MS acquisition modes (e.g., DDA and DIA).

Quality assurance and quality control for UHPLC-HRMS analysis

The extraction solution of fused silica (Corning 7980 0F, Edmund) was prepared in parallel with the meteorite samples as a procedural blank to monitor potential contamination during the entire sample preparation stage.[4,8] A solvent blank was also included. Comparisons between solvent and procedural blanks showed consistent ion detection and intensity (Figure S7), indicating that no additional contamination was introduced during sample preparation. However, terrestrial contamination during meteorite collection and storage cannot be completely excluded, highlighting the unique value of pristine extraterrestrial materials returned by sample-return missions. All reagents used were LC-MS grade from Fisher Chemical.

For UHPLC-HRMS analysis, 10 μL from each meteorite extract was pooled to generate a quality control (QC) sample. This pooled QC was injected every ten runs, resulting in a total of seven QC injections. The total ion chromatograms (TICs) of the QC samples remained stable throughout the sequence. Partial least squares discriminant analysis (PLS-DA) showed a tight clustering of the pooled QC samples, indicating acceptable analytical reproducibility (Figure 4). Compounds with a relative standard deviation (RSD) below 40% in the pooled QC were retained,[58] while those with high abundance in the blank were removed.

UHPLC-HRMS data processing

A total of 2,809 compounds (Data S1) were ultimately selected for downstream omics-based statistical analysis.[33] Kendrick mass defect (KMD) plots[59] were used to visualize the SOM compounds in meteorites (Figure S7). Data were acquired in DIA mode, which enabled the analysis of compound structures via MS^2 spectra (Figure S8). However, the obtained MS^2 spectra did not exactly match entries or theoretical fragmentation patterns[60] in current spectral databases (Table S1). In silico predictions of some compounds did yield apparent matches, but the prevalence of numerous structural isomers, in conjunction with the limited number of diagnostic fragment ions, precluded confident structural assignment of the compounds. While some MS^2 fragments displayed similarities (Figure S8), indicating common chemical substructures, full structural elucidation based on MS^2 data alone remains challenging. Although meteorite samples provide a larger available material compared to asteroid samples, isolating and purifying individual SOM compounds through preparative chromatography followed by nuclear magnetic resonance (NMR) analysis remains technically difficult and cost-prohibitive. Under these constraints, the analysis was restricted to molecular formula assignment in Progenesis QI, using the following elemental ranges: C 0-100, H 0-100, N 0-10, O 0-20, and S 0-2, with a minimum isotope pattern similarity threshold of 60%. Nevertheless, omics approaches enable robust comparative analysis of SOM abundance across meteorites.

Based on the PLS-DA (Figure 4), differential markers were identified using a Variable Importance in the Projection (VIP) threshold > 1. Molecular formulas

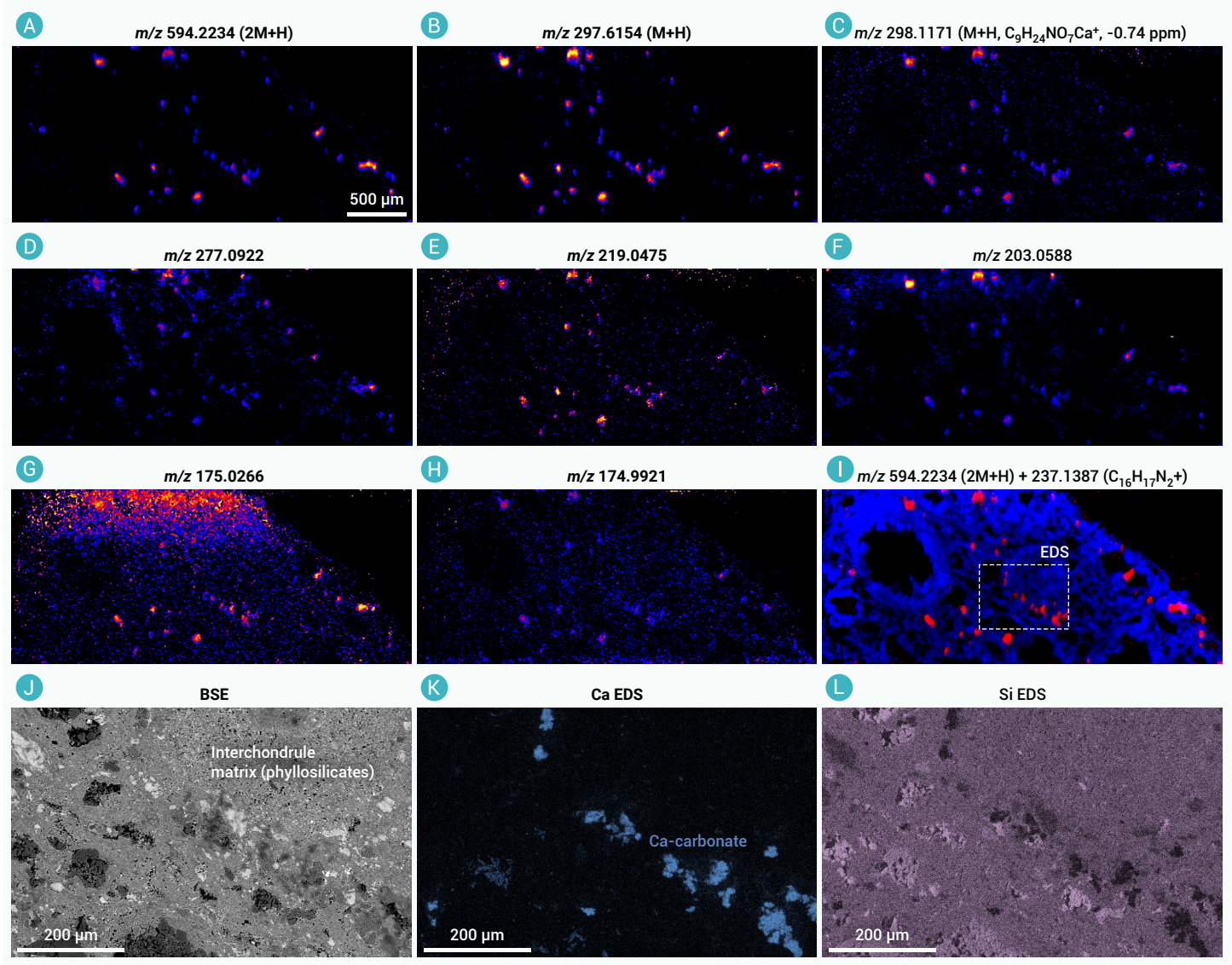

Figure 3. The DESI-HRMS imaging of molecules related to carbonates in the Murchison meteorite (A-H) Ions enriched in carbonates. (I) Combination image of an ion related to carbonates (red) and an ion related to phyllosilicates (blue). (J-L) BSE and EDS maps of the dashed box in panel (I).

were assigned to 380 compounds (Data S1) with a mass error < 1 ppm and isotopic pattern. These SOM markers are predominantly composed of CHN, CHNO, CHOS, and CHO species, consistent with previous studies.[1,3]

In the heatmap (Figure 5), to mitigate inter-sample variation in ion response, peak areas were normalized by calculating Z-score.

$$z = \frac{X - \mu}{\sigma}$$

Where X is the observed value (e.g., SOM abundance in a given meteorite), μ is the dataset mean, and σ is the standard deviation. Z-score scandalization was applied solely for multivariate visualization and not for quantitative comparisons.[61] The raw abundances are provided in Data S1.

RESULTS AND DISCUSSION

Spatial Distribution of SOM

Due to solvent extraction selectivity, ionization efficiency, and matrix effects, DESI-HRMS signal intensities cannot be directly compared between different samples.[31] However, within the same sample, DESI-HRMS imaging at a spatial resolution of ~10 μm (Figure S3) co-localized with mineralogical maps (BSE) enables visualization of the relative distribution of methanol-extractable (primarily polar) organic matter among different mineral phases and microstructures (Figures 1-3). This approach reveals mineral-scale spatial heterogeneity in SOM abundance and composition.

In positive ion mode, solvent-related background ions are commonly present in DESI-HRMS spectra (Figure S4). In this study, SOM was not detected by DESI-HRMS in the Allende, Zag, Ningqiang, and Orgueil meteorites. The absence of detectable SOM in Orgueil can be attributed to the combined effects of its highly porous substrate[62] and differences in SOM abundance.[26] The KMD plot shows CHN, CHNO and CHOS homologues, as well as CHO species in CM chondrites, consistent with previous reports.[26,31] By comparison, the KMD pattern of SOM in Tarda was distinctly different from that of the CM chondrites (Figure S5). However, because of the polarity selectivity of DESI ionization and matrix effects discussed above, we do not directly compare DESI-HRMS signal intensities or profiles across different samples.

Phyllosilicates and carbonates are both secondary minerals produced during aqueous alteration.[63] The co-localization of DESI-HRMS imaging with BSE images (Figure 1) reveals that SOM is dispersed throughout the matrix of the meteorite, showing a direct spatial association with aqueously altered phyllosilicate minerals, whereas carbonate domains generally exhibit low SOM abundance. In the Tarda meteorite, which lacks intact chondrules, SOM is evenly distributed in the phyllosilicate matrix (Figure 1E). Conversely, in other CM chondrites, the distribution of SOM within phyllosilicates is heterogeneous, with SOM being notably concentrated around the outer edges of chondrules, especially in their fine-grained rims (FGRs). The spatial distribution of most SOM compounds (CHN, CHNO and CHOS) remains consistent

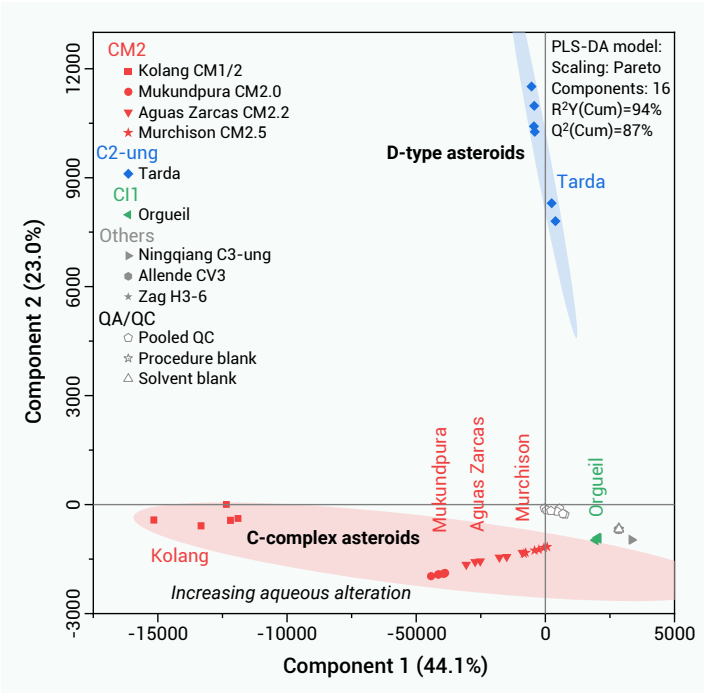

Figure 4. Partial least squares-discriminant analysis (PLS-DA) of 2,809 SOM compounds detected by UHPLC-HRMS Ellipses indicate the 95% confidence ellipses for the CM chondrites and Tarda meteorite.

(Figures S9-S10), except for a few ions related to carbonate (Figure 3).

Using the Murchison meteorite as an example, we selected multiple regions of interest within four representative mineralogical or structural domains and extracted the corresponding DESI-HRMS spectra for statistical analysis (Figure 2). The peak intensities in the DESI-HRMS spectra (Figure 2A) and the distributions of normalized SOM abundances summarized in the violin plots (Figure 2C) indicate that, phyllosilicates in FGRs generally exhibit a higher abundance of SOM compared to those present in the interchondrule matrix although SOM within individual FGRs is heterogeneous. Additionally, the SOM contrast between the FGRs and matrix is real rather than a matrix-effect artifact, because even in the raw (uncorrected) images the internal standard (leucine enkephalin) does not exhibit higher response in the FGRs, whereas SOM shows intrinsically higher signal intensity (Figure S6). The molecular compositions of SOM in FGR and interchondrule-matrix phyllosilicates are broadly similar, with differences dominated by abundance rather than by distinct SOM families.

In contrast, Ca-carbonate phases show significant depletion of SOM (Figure 2), with only a few specific molecules being enriched (Figures 3 & S11). This contrast between Ca-carbonate and phyllosilicates is clearly captured by the PCA plot based on SOM compositions and abundances (Figure 2D). No SOM was detected in unaltered olivine within chondrules, where the signals are indistinguishable from the solvent background (Figures 2A & S4). This result is consistent with previous DESI imaging observations in Murchison.[31] We infer that the variations in SOM abundance and composition across different minerals or structural domains are genuine rather than artifacts of matrix effects, because carbonates show both enrichments and depletions of SOM compared with phyllosilicates (Figure 3). At present, molecular formulas have not been assigned to the ions enriched in Ca-carbonate, as the specific form of the parent ion addition and the potential involvement of metal elements remain uncertain. Nevertheless, the absence of these carbonate-associated ions from both solvent and procedural blank spectra indicates that they are unlikely originated from laboratory contamination.

Associations between SOM and Mineral Phases

The spatial correlation between SOM and phyllosilicates (Figure 1) indicates a coupled process of SOM synthesis and mineral alteration during aqueous alteration. In carbonaceous chondrite parent bodies, this coupling is plausibly facilitated by the serpentinization of anhydrous silicates, whereby infiltrating aqueous fluids transform olivine- and pyroxene-rich assemblages into phyllosilicates and, in the process, generate H_2 and modify fluid pH and redox state.[64] The layered structure and surface hydroxyl groups of water-rich phyllosilicates may serve as active sites for SOM adsorption and preservation.[25,65-67] Experimental studies have demonstrated that water–rock reactions in the presence of phyllosilicates have the capacity to synthesize complex organic solids from simple precursors, as well as to govern the hydrothermal transformation pathways and the functional group composition of organic matter.[68,69]

The heterogeneous distribution of SOM in CM chondrites and the enrichment of SOM in FGRs (Figures 1-2) suggest that SOM may have been redistributed by aqueous fluid mobilization. FGRs are chemically similar to the fine-grained matrix but have more compact textures and lower porosity.[70] The origin of FGRs remains debated, with two scenarios most frequently proposed:[71,72] (i) nebular dust accretion, in which FGRs are hypothesized to have formed via a dust-accretion process analogous to that responsible for the fine-grained matrix,[70,71] and (ii) formation on the parent-body via regolith compaction[70] and associated processing.[73,74] Nebular dust accretion alone does not straightforwardly account for the pronounced contrast in SOM abundance observed between FGRs and the matrix (Figure 2), suggesting that additional parent-body processes may be required. Moreover, because no steep thermal gradient has been observed within CM parent bodies at the microscale during aqueous alteration,[75,76] the enrichment of SOM in FGRs is unlikely to be simply attributable to local temperature variations.

A more concise explanation is that aqueous alteration involved fluid transport,[63] during which SOM was intercepted by chondrules or other low-permeability minerals, leading to SOM accumulation in FGRs with smaller grain size[74] and higher high surface area. Notably, SOM is absent in unaltered chondrules (ROI2 in Figure 1A) but appears in partially altered chondrules (ROI1 in Figure 1A), though at a lower abundance than in the FGRs. This observation further supports the notion that progressive aqueous alteration and fluid activity drive changes in SOM distribution.[25,28,29,77] Given the approximately non-directional enrichment of SOM around FGRs, a strongly unidirectional flow of the aqueous fluids is improbable. This finding aligns with the convecting mudball hypothesis,[75] which proposes that the system was thoroughly mixed with nebular fines, ice, and chondrules. Therefore, at least on the millimeter scale observed through DESI-HRMS imaging, the redistribution of SOM could be driven by fluid movement[76,78] during aqueous alteration in a locally open system.

The difference in SOM composition and abundance between carbonate and phyllosilicates have two possible explanations. In the multi-step aqueous alteration,[79] changes in fluid properties between the formation of phyllosilicates and carbonates (e.g., Type 2 calcite[63,80]) might lead to the depletion of most SOM species in carbonate phases (Figure 2) and help explain why ions enriched in carbonates are absent in phyllosilicates (Figures 3 & S11). In addition, differences in the crystal-chemical structures between carbonates and phyllosilicates likely result in distinct adsorption mechanisms for SOM, with phyllosilicates being more favorable for most SOM adsorption and preservation, whereas carbonates may exhibit a strong affinity for specific ions (Figure 3). However, potential differences in SOM among various types of carbonates[63,80] require further investigation, preferably through the establishment of spatial correlations between DESI-HRMS imaging and in situ measurements of carbonate isotopic compositions.

Compositional Diversity of SOM among Meteorites

The incorporation of UHPLC-HRMS provides a complement to DESI-HRMS, enabling direct comparison of SOM composition and abundance between samples. Although it remains difficult to unequivocally identify SOM structures based solely on MS^2 spectra in this study (Figure S8), the addition of retention time as a chromatographic dimension offers valuable structural insights. UHPLC-HRMS analysis detected 2,809 SOM compounds (Data S1) in methanol extracts of nine meteorites, thereby enabling subsequent omics-based statistical analysis (Figures 4-6).

Under the current BEH C18 column and ESI(+) analysis conditions, SOM is predominantly composed of CHN, CHNO, CHOS homologues, and CHO compounds (Data S1). These formula families broadly correspond to suites

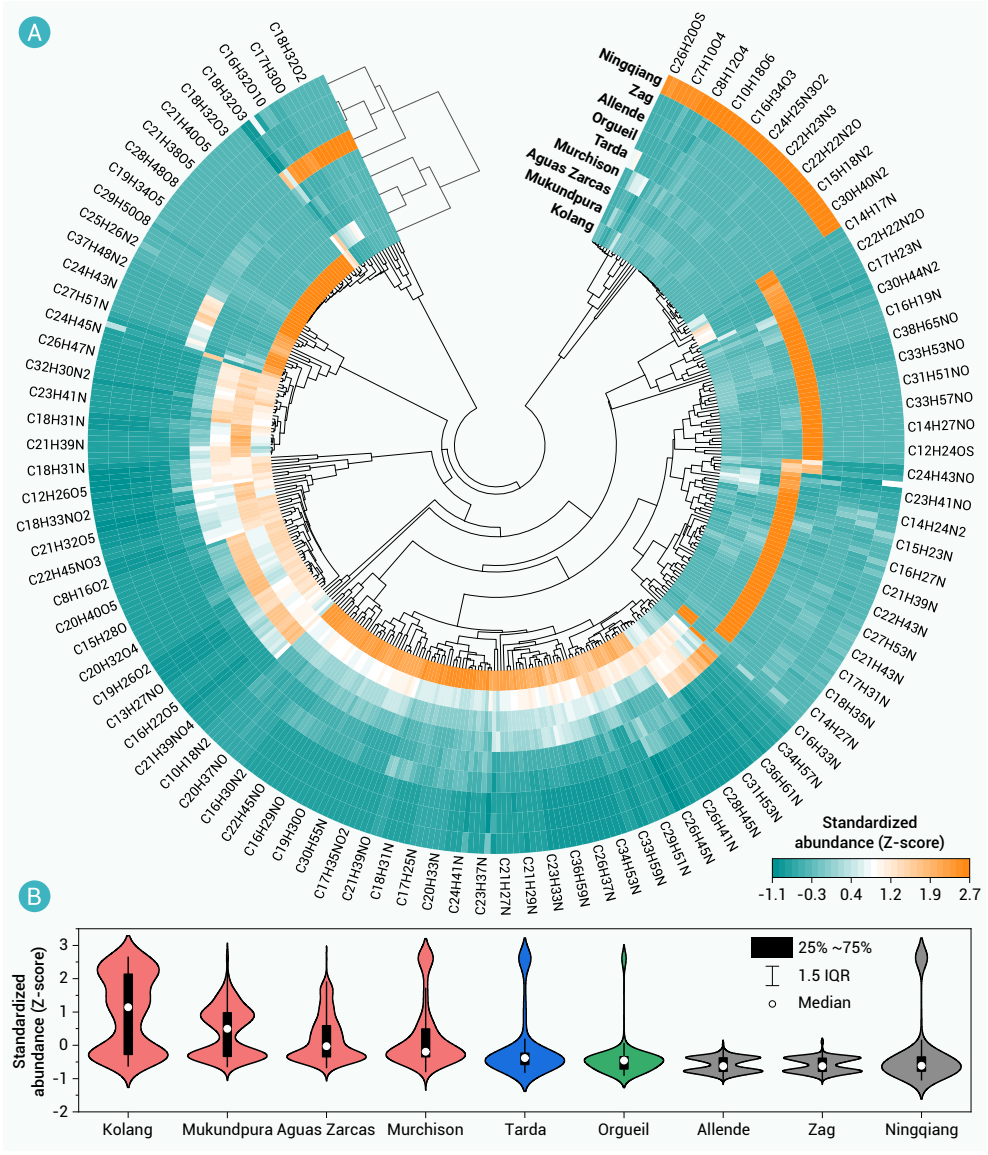

Figure 5. Differential SOM markers across meteorites (A) Circular heatmap for the Z-score standardized abundances of 380 differential SOM markers across meteorites. Hierarchical clustering is applied to both markers and meteorite samples, and dendrograms indicate similarity patterns. (B) Violin plots for the distribution of Z-score standardized abundances of the differential markers in each meteorite.

of aliphatic and aromatic amines, and N-heterocycles (CHN, CHNO), oxygenated hydrocarbons such as aldehydes, alcohols, and carboxylic-acid–derived species (CHO), and organosulfur compounds.[3,25,27-29,81,82] In the PLS-DA plot (Figure 4), the cumulative Q^2 increased to 0.87 with 16 components, indicating substantial predictive ability under cross-validation, while the cumulative R^2Y reached 0.94. The statistics thus provide a robust multivariate framework for resolving systematic differences in SOM composition and abundance among the meteorites. The Allende CV3 and Zag H3-6 meteorites overlap with the solvent and procedure blanks, indicating no detectable SOM in the methanol extracts of these meteorites (Figure S7). The distribution patterns of the four CM chondrites in PLS-DA correlate with their extent of aqueous alteration. Cluster analysis (Figure 5A) further indicates that SOM in these four CM chondrites was compositionally similar. Kolang CM1/2, which experienced the most extensive aqueous alteration, exhibited the highest abundances of most CHN, CHNO, and CHOS differential markers (Figures 5 & S12), followed by Mukundpura CM2.0, Aguas Zarcas CM2.2, and Murchison CM2.5.

Notably, the separation of CM chondrites and Tarda C2-ung into two distinct groups (Figure 6) indicates significant differences in their organic compositions. Although the m/z values of compounds (MS^1) in Tarda were consistent with those in CM chondrites, the compounds in Tarda C2-ung had longer retention times (Figures 6C-D) and distinct MS^2 spectra, indicating differences in isomeric composition and the presence of less polar organic molecules. This polarity difference between Tarda C2-ung and CM chondrites also explains the divergent KMD patterns observed in DESI-HRMS analysis (Figure S6), as the less polar SOM in Tarda C2-ung is more difficult to ionize under DESI conditions.[83]

The Ningqiang C3-ung meteorite was positioned on the opposite side of the CM chondrites in the PLS-DA plot (Figure 4), with a higher abundance of CHO compounds and marked depletion of CHN species (Figure S12B). The abundance of CHNO and CHN compounds in Orgueil was much lower than those in CM chondrites (Figure S12). In contrast, several CHO markers were detected in Orgueil but were absent in CM chondrites (Figures 5A & S12B). These results agree with previous DESI-HRMS comparisons between Orgueil and Murchison, which reported that Orgueil is enriched in CHO but depleted in CHN/CHNO compounds.[28]

Associations between SOM and Parent Body Conditions

The composition of SOM in different meteorite types reflects the controls exerted by parent-body conditions. CI and CM carbonaceous chondrites represent two distinct chemical groups, primarily defined by systematic differences in their bulk chemistry, mineralogy and characteristic oxygen-isotope systematics,[84] which are commonly interpreted to reflect accretion from different nebular reservoirs and evolution on different parent bodies.[85] The similarity in SOM composition among the four CM chondrites (Figure 5A) is consistent with their shared classification and also suggests that they may have originated from a common precursor and experienced a similar organic synthesis pathway.

CM-type chondrites with higher levels of aqueous alteration show higher mean standardized abundances (Figure 4C), indicating that aqueous alteration promotes the synthesis of CHN, CHNO, and CHOS compounds in CM chondrites. The trends in SOM composition revealed by UHPLC-HRMS are consistent with previous FT-ICR/MS observations[24] that compare the relative abundances of classes such as CHN and CHO across meteorites with different degrees of aqueous alteration. Although the PLS-DA results based on UHPLC-HRMS differ from those from FT-ICR/MS[24,26] because UHPLC adds a retention-time dimension that carries structural information, both analysis reveal the influence of alteration degree or temperature[26] on the evolution of SOM. As the extent of alteration increases in CM chondrites, Fe valence is observed to decrease from 2.60 to 2.40,[86] which correlates with the increasing abundance of CHN compounds (Figure S12D). CHO compounds, on the other hand, are predominantly detected in the Murchison CM2.5 meteorite (Figure S12B).

Although Orgueil is thought to have undergone the highest degree of aqueous alteration, its SOM abundance is lower than that of CM-type chondrites (Figure 5B), suggesting that Orgueil and CM chondrites likely originated from different parent asteroids[87-89] and underwent different aqueous alteration processes. A similar discrepancy is observed in the amino acid composition and abundance of Orgueil meteorite compared to CM chondrites.[10,90] The amino acid abundance in Orgueil is about one-third of that detected in CM

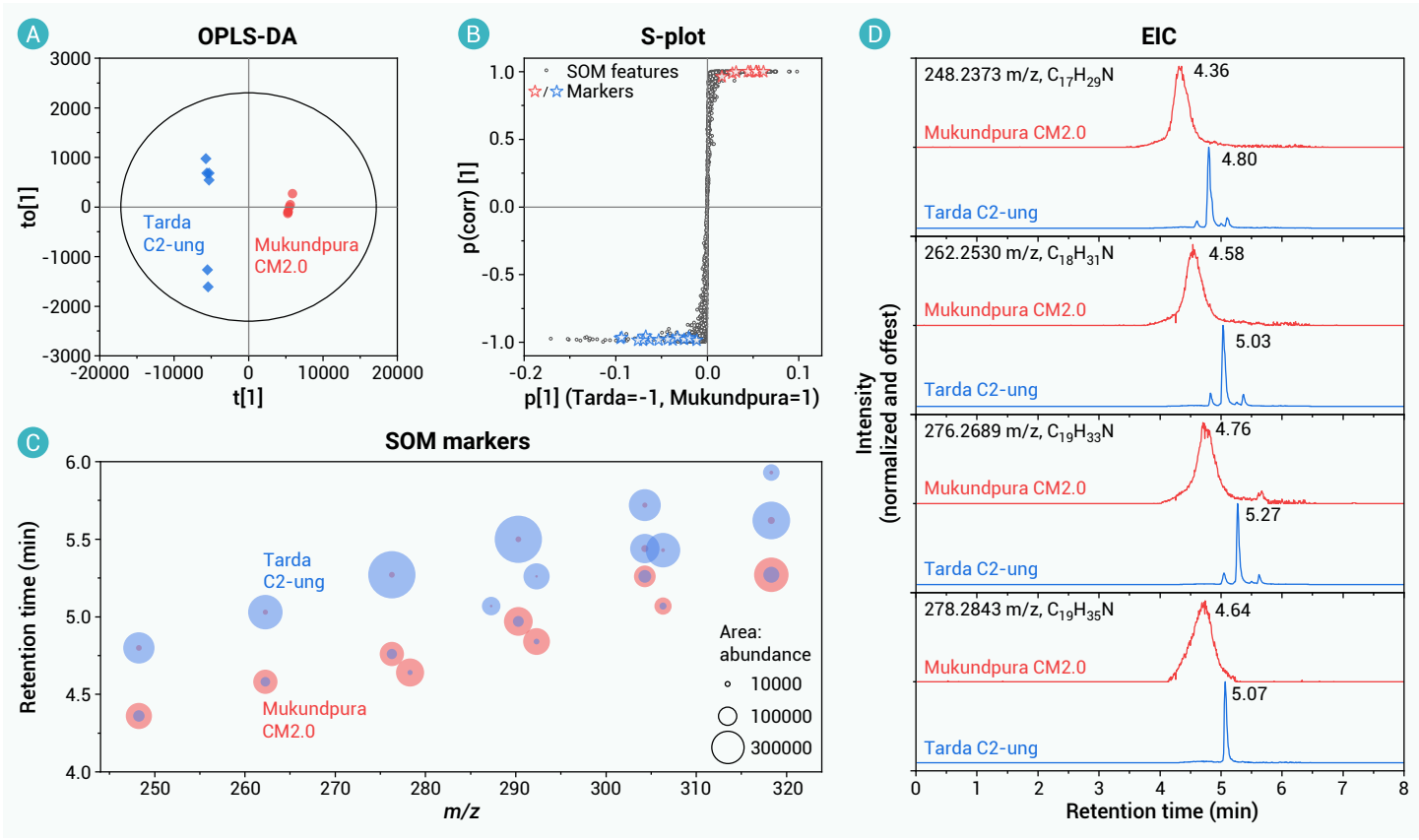

Figure 6. SOM differences between the Tarda C2-ung and Mukundpura CM2.0 meteorites revealed by UHPLC–HRMS (A) OPLS-DA score plot of SOM features, with the 95% confidence ellipse. (B) S-plot for SOM compounds, and differential markers are highlighted. (C) *m/z*–retention time map of the differential markers highlighted in (B). (D) Extracted ion chromatograms (EICs) of representative markers.

chondrite. In addition, the SOM abundance in the CI chondrite-like Ryugu asteroid is lower than that in Murchison.[3] The Orgueil meteorite exhibits a higher Fe valence state (2.77) relative to CM chondrites (2.60–2.40)[86] and a lower Fe/S ratio (0.85) relative to CM chondrites (0.89–0.97),[45] indicating that aqueous alteration in Orgueil occurred under more oxidizing conditions. In line with this, the presence of CHO compounds in Orgueil (Figures 5A & S12B) suggests that the redox state during aqueous alteration can significantly influence SOM composition.[91] Recent laboratory simulations have demonstrated that asteroidal aqueous alteration can actively deplete and transform amino acids, with hydrothermal and redox-driven electrochemical processes modifying their abundances, stability, and isomeric distributions.[69,92] Notably, a recent study suggested that the highly oxidized state of Orgueil may result from terrestrial oxidative alteration.[93] This highlights the need for future SOM studies to include multiple CI chondrites, particularly the recently discovered Oued Chebeika 002 meteorite.

The influence of fluid redox conditions is further illustrated by the SOM in the Ningqiang (C3-ung) meteorite. Previous mineralogical[41] and oxygen-isotope[94] studies of opaque assemblages and magnetite in Ningqiang meteorite have indicated that pre-existing metal phases were oxidized by aqueous fluids on the parent body, thereby corroborating our observation that SOM in Ningqiang are dominated by CHO compounds (Figures 5A & S12B) .

The SOM difference between Tarda and CM chondrites (Figures 4-6) is likely attributable to their parent asteroids. CM chondrites are suggested to originate from C-complex asteroids in the main belt (2.1-3.3 AU),[95] while Tarda is thought to come from more remote D-type asteroids[46,47] in the outer main belt and Jupiter Trojan regions (~ 5.2 AU).[95] Dynamical models and ^{13}C isotope have suggested that the initiation of C-complex asteroids originally formed beyond 5 AU,[95,96] whereas D-type asteroids accreted at even greater heliocentric distances of > 10 AU. The reflectance spectra (0.4-2.5 μm, VNIR band) of D-type asteroids show no absorption features but a very steep slope,[97] which has been interpreted as indicating either structurally simpler organic compounds or altered chromophores in complex molecules.[47,98] A shortening of the conjugated system in organic molecules would cause a blue shift of the absorption peak, thereby eliminating distinct absorbance features in the VNIR region. These observations imply a potential link between SOM polarity (e.g., isomerism), structural characteristics (e.g., conjugation length), and reflectance spectra. Consequently, it can be hypothesized that the heliocentric distance associated with an asteroid's source region and subsequent migration history exerts an influence on its temperature,[95] which in turn affects the pathways of organic synthesis. However, further studies on samples from diverse asteroids, particularly additional D-type samples, are required to verify this mechanism.

The absence of detectable SOM in the Allende CV3 meteorite (Figures 4-5) is most likely attributed to its history of thermal metamorphism at temperatures of 550–590°C, followed by subsequent alteration at temperatures below 300°C.[99] The intense thermal metamorphism would have destroyed potentially pre-existing SOM, while the subsequent limited alteration—reflected by Allende's largely anhydrous mineralogy[40]—was insufficient to promote the synthesis of new, complex SOM. This finding is consistent with previous studies that also failed to detect amino acids in Allende,[100] suggesting that minimal alteration cannot facilitate the formation of complex SOM. The absence of detectable SOM in the Zag meteorite is consistent with its classification as an ordinary chondrite that has undergone varying degrees of thermal metamorphism.[39]

Multiscale Controls on SOM Evolution: From Solar System to Microscale

Previous studies establish a continuous framework for SOM evolution,[14] spanning the irradiation of interstellar ices[16,19] in the ISM,[15-17] subsequent accretion[2,14] and radial migration of parent bodies, and later parent-body processing.[3,5,101] Our results suggest that controlling mechanisms can be understood at three spatial scales: the Solar System, the parent body, and the microscale (Figure 7).

At the Solar System scale (Figure 7A), the heliocentric distance for the source regions of asteroid parent bodies influences their ambient temperature, water/rock ratio, and initial inventory of organic precursors.[95,96] These environmental factors, set by orbital distance and dynamical history, dictate

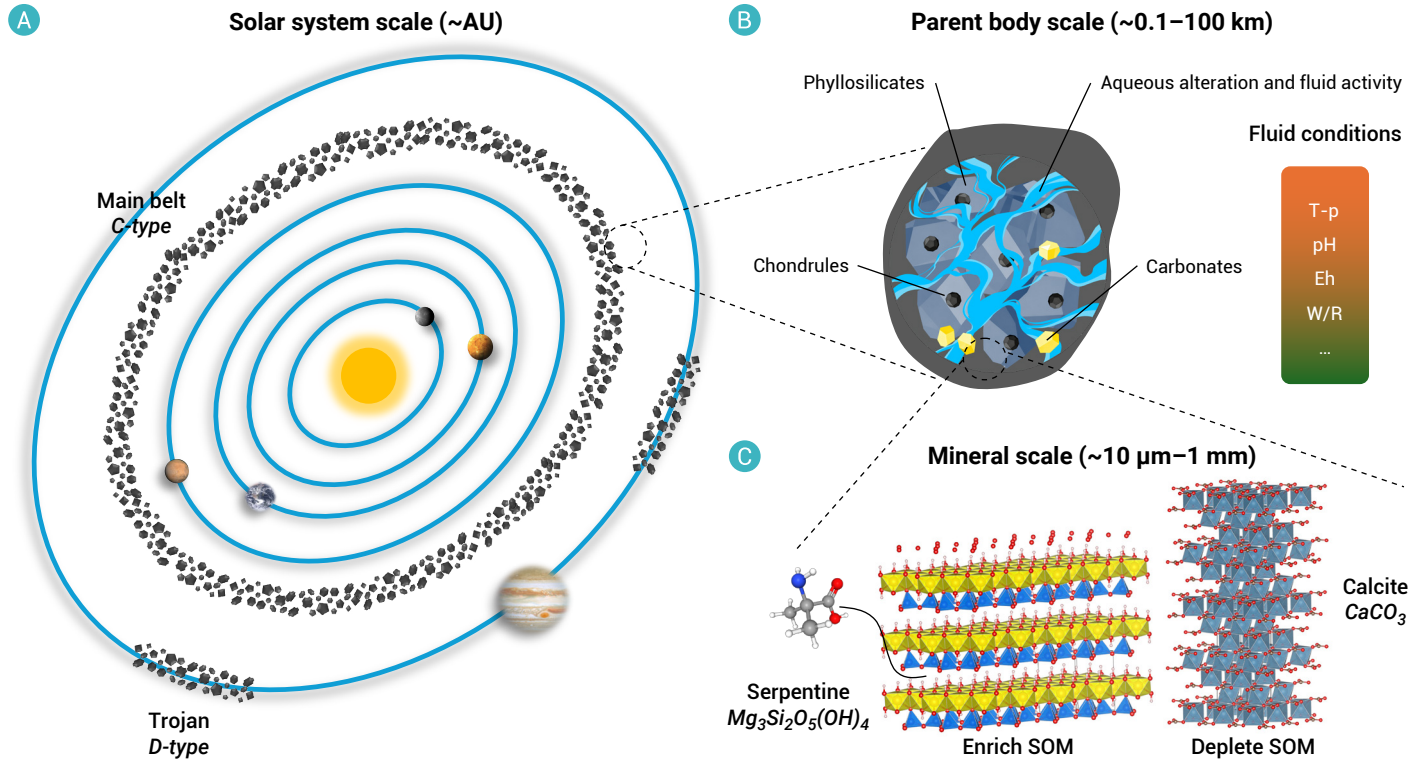

Figure 7. Multiscale controls on the evolution of SOM in carbonaceous chondrites (A) The Solar System scale—parent body source regions set the global environment. (B) The parent body scale—fluid conditions influence the dominant molecular composition. (C) The microscale—mineral structures such as serpentine and calcite regulate SOM adsorption and retention.

the pathways and outcomes of SOM synthesis. For instance, differences in polarity and isomeric diversity (Figure 6) between the Tarda and CM chondrites are likely linked to the distinct source regions of their parent bodies.

At the parent-body scale (Figure 7B), coupled fluid conditions govern the elemental composition and molecular types of SOM formed, including temperature, pH–alkalinity, redox state, water–rock ratio, and ionic composition/speciation. Reducing environments tend to favor the synthesis and preservation of CHN compounds,[35,102,103] whereas more oxidizing conditions may favor the formation of organic acids,[35] consistent with our observations of SOM differences between Orgueil and CM chondrites (Figure 5). The recent detection of sugars in Bennu samples,[13] together with their relatively alkaline extract pH (8.23), further highlights the role of pH in shaping organic inventories.

At the microscale (Figure 7C), the distribution and preservation of SOM are influenced by the crystalline structure, surface chemistry, and porosity of the dominant mineral phases. Phyllosilicates (e.g., serpentine) provide extensive interlayer spacing and surface hydroxyls, facilitating the adsorption, complexation, and retention of organic molecules.[65-67] In contrast, carbonate minerals are generally depleted in SOM (Figure 2). Laboratory simulations demonstrated that mineral type, degree of crystallinity, and nanoscale structure significantly influence the efficiency of SOM accumulation and preservation (e.g., amino acids and nucleobases).[69,104] Moreover, dense silicate minerals (such as olivine and pyroxene) within chondrules may impede fluid flow, resulting in preferential enrichment of SOM in the FGRs surrounding chondrules, thereby reflecting the control of mineral physical properties on the SOM spatial distribution. This pattern constrains a lower bound on the fluid transport distance,[76] indicating fluid movement over at least several hundred micrometers during ~3 Myr of aqueous alteration.[78]

The controlling factors at different scales are not isolated but rather mutually interconnected. The Solar System-scale environment establishes the boundary conditions for fluid properties within the parent body, which in turn influences both the mineralogical context[105] and organic synthesis. Ultimately, mineralogical controls at the microscale dictate the spatial heterogeneity and preservation potential of SOM.

This multiscale framework (Figure 7) takes interstellar ices as the starting point for SOM evolution and focuses on the synthesis of SOM from simple to more complex molecules.[106] It does not treat IOM as an initial reservoir, nor does it explicitly consider the breakdown of IOM during aqueous alteration[107] and the associated release of SOM.[6,108] This framework is not incompatible with previous observations from the Tagish Lake meteorite, which indicate that SOM can be simplified during aqueous alteration.[109] If the system experienced further heating,[110] more extensive aromatization and a partial transformation of SOM into IOM are chemically plausible,[111-113] reducing the abundance and structural diversity of the remaining SOM. Future investigations of SOM evolution should consider its relationship with IOM by jointly quantifying the occurrence, abundance and composition of both SOM and IOM in experimental simulations and samples.

CONCLUSIONS

DESI-HRMS imaging reveals that the distribution of SOM in carbonaceous chondrites exhibits significant heterogeneity at the microscale. SOM is predominantly distributed in phyllosilicates and is enriched in fine-grained rims of chondrules, indicating that its distribution is jointly controlled by mineral hosts and microstructures. UHPLC-HRMS results further indicate the presence of systematic differences in SOM abundance and heteroatom-class composition among the various groups of chondrites. These variations can be attributed to differences in the source regions and fluid conditions of the parent bodies. In summary, the formation, evolution, and preservation of SOM in carbonaceous chondrites are influenced by the Solar System environment, the parent body processes, and microscale mineral phases. Aqueous alteration and associated fluid activity constitute the key driving forces, shaping both the molecular complexity and the heterogeneous distribution of extraterrestrial organic matters.

REFERENCES

1. Schmitt-Kopplin P., Gabelica Z., Gougeon R. D., et al. (2010). High molecular diversity of extraterrestrial organic matter in Murchison meteorite revealed 40 years after its fall. *Proc. Natl. Acad. Sci. USA.* **107**:2763–2768. DOI:10.1073/pnas.0912157107
2. Chan Q. H. S., Nomura H., Kebukawa Y., et al. (2025). Organic matter - From birth in the interstellar medium and beyond to incorporation and processing in planetary

building blocks. In Reference Module in Earth Systems and Environmental Sciences (Elsevier), pp:147-202. DOI:10.1016/b978-0-323-99762-1.00145-5
3. Naraoka H., Takano Y., Dworkin J. P., et al. (2023). Soluble organic molecules in samples of the carbonaceous asteroid (162173) Ryugu. *Science* **379**:1–11. DOI:10.1126/science.abn9033
4. Glavin D. P., Dworkin J. P., Alexander C. M. O., et al. (2025). Abundant ammonia and nitrogen-rich soluble organic matter in samples from asteroid (101955) Bennu. *Nat. Astron.* **9**:199–210. DOI:10.1038/s41550-024-02472-9
5. Yabuta H., Cody G. D., Engrand C., et al. (2023). Macromolecular organic matter in samples of the asteroid (162173) Ryugu. *Science* **379**:1–13. DOI:10.1126/science.abn9057
6. Pizzarello S., Davidowski S. K., Holland G. P., et al. (2013). Processing of meteoritic organic materials as a possible analog of early molecular evolution in planetary environments. *Proc. Natl. Acad. Sci. USA* **110**:15614–15619. DOI:10.1073/pnas.1309113110
7. Ehrenfreund P. and Cami J. (2010). Cosmic carbon chemistry: From the interstellar medium to the early Earth. *Cold Spring Harb. Perspect. Biol.* **2**:a002097. DOI:10.1101/cshperspect.a002097
8. Oba Y., Takano Y., Furukawa Y., et al. (2022). Identifying the wide diversity of extraterrestrial purine and pyrimidine nucleobases in carbonaceous meteorites. *Nat. Commun.* **13**:1–10. DOI:10.1038/s41467-022-29612-x
9. Herd C. D., Blinova A., Simkus D. N., et al. (2011). Origin and evolution of prebiotic organic matter as inferred from the Tagish Lake meteorite. *Science* **332**:1304–1307. DOI:10.1126/science.1203290
10. Ehrenfreund P., Glavin D. P., Botta O., et al. (2001). Extraterrestrial amino acids in Orgueil and Ivuna: tracing the parent body of CI type carbonaceous chondrites. *Proc. Natl. Acad. Sci. USA* **98**:2138–2141. DOI:10.1073/pnas.051502898
11. Cooper G., Kimmich N., Belisle W., et al. (2001). Carbonaceous meteorites as a source of sugar-related organic compounds for the early Earth. *Nature* **414**:879–883. DOI:10.1038/414879a
12. Furukawa Y., Chikaraishi Y., Ohkouchi N., et al. (2019). Extraterrestrial ribose and other sugars in primitive meteorites. *Proc. Natl. Acad. Sci. USA* **116**:24440–24445. DOI:10.1073/pnas.1907169116
13. Furukawa Y., Sunami S., Takano Y., et al. (2025). Bio-essential sugars in samples from asteroid Bennu. *Nat. Geosci.* **19**:19–24. DOI:10.1038/s41561-025-01838-6
14. Potiszil C., Yamanaka M., Sakaguchi C., et al. (2023). Organic matter in the asteroid Ryugu: What we know so far. *Life (Basel)* **13**:1–13. DOI:10.3390/life13071448
15. Bernstein M. P., Dworkin J. P., Sandford S. A., et al. (2002). Racemic amino acids from the ultraviolet photolysis of interstellar ice analogues. *Nature* **416**:401–403. DOI:10.1038/416401a
16. Javelle T., Ruf A., Bouquet A., et al. (2024). Impact of environmental conditions on organic matter in astrophysical ice analogues. *Mon. Not. Roy. Astron. Soc.* **534**:2305–2313. DOI:10.1093/mnras/stae2186
17. Danger G., Vinogradoff V., Matzka M., et al. (2021). Exploring the link between molecular cloud ices and chondritic organic matter in laboratory. *Nat. Commun.* **12**:1–9. DOI:10.1038/s41467-021-23895-2
18. Taniguchi K., Gorai P. and Tan J. C. (2024). Carbon-chain chemistry in the interstellar medium. *Astrophys. Space Sci.* **369**:1–41. DOI:10.1007/s10509-024-04292-9
19. Ligterink N. F. W., Pinilla P., van der Marel N., et al. (2024). The rapid formation of macromolecules in irradiated ice of protoplanetary disk dust traps. *Nat. Astron.* **8**:1257–1263. DOI:10.1038/s41550-024-02334-4
20. Stalport F., Rouquette L., Poch O., et al. (2019). The photochemistry on space station (PSS) experiment: Organic matter under Mars-like surface UV radiation conditions in low Earth orbit. *Astrobiology* **19**:1037–1052. DOI:10.1089/ast.2018.2001
21. Portugal W., Pilling S., Boduch P., et al. (2014). Radiolysis of amino acids by heavy and energetic cosmic ray analogues in simulated space environments: α-glycine zwitterion form. *Mon. Not. Roy. Astron. Soc.* **441**:3209–3225. DOI:10.1093/mnras/stu656
22. Micelotta E. R., Jones A. P. and Tielens A. G. G. M. (2010). Polycyclic aromatic hydrocarbon processing in interstellar shocks. *Astron. Astrophys.* **510**:1–19. DOI:10.1051/0004-6361/200911682
23. Peterson E., Horz F. and Chang S. (1997). Modification of amino acids at shock pressures of 3.5 to 32 GPa. *Geochim. Cosmochim. Acta* **61**:3937-3950. DOI:10.1016/s0016-7037(97)00192-0
24. Laurent B., Maillard J., Afonso C., et al. (2022). Diversity of chondritic organic matter probed by ultra-high resolution mass spectrometry. *Geochem. Perspect. Lett.* **22**:31–35. DOI:10.7185/geochemlet.2224
25. Potiszil C., Tanaka R., Ota T., et al. (2020). Concentration of meteoritic free organic matter by fluid transport and adsorption. *Geochem. Perspect. Lett.* **13**:30–35. DOI:10.7185/geochemlet.2010
26. Schmitt-Kopplin P., Hertkorn N., Harir M., et al. (2023). Soluble organic matter Molecular atlas of Ryugu reveals cold hydrothermalism on C-type asteroid parent body. *Nat. Commun.* **14**:1–9. DOI:10.1038/s41467-023-42075-y
27. Hashiguchi M. and Naraoka H. (2018). High - mass resolution molecular imaging of organic compounds on the surface of Murchison meteorite. *Meteorit. Planet. Sci.* **54**:452–468. DOI:10.1111/maps.13211
28. Hashiguchi M., Aoki D., Fukushima K., et al. (2023). The spatial distribution of soluble organic matter and their relationship to minerals in the asteroid (162173) Ryugu. *Earth Planets. Space.* **75**:1–25. DOI:10.1186/s40623-023-01792-w
29. Naraoka H. and Hashiguchi M. (2018). In situ organic compound analysis on a meteorite surface by desorption electrospray ionization coupled with an Orbitrap mass spectrometer. *Rapid Commun. Mass Spectrom.* **32**:959–964. DOI:10.1002/rcm.8121
30. Nakamura E., Kobayashi K., Tanaka R., et al. (2022). On the origin and evolution of the asteroid Ryugu: A comprehensive geochemical perspective. *Proc. Jpn. Acad. Ser. B Phys. Biol. Sci.* **98**:227–282. DOI:10.2183/pjab.98.015
31. Dong M., Yang W., Hao J., et al. (2025). Cross-scale multimodal imaging for organic matter in extraterrestrial samples. *Anal. Chem.* **97**:8258–8267. DOI:10.1021/acs.analchem.4c05804
32. Perez de Souza L., Alseekh S., Scossa F., et al. (2021). Ultra-high-performance liquid chromatography high-resolution mass spectrometry variants for metabolomics research. *Nat. Methods* **18**:733–746. DOI:10.1038/s41592-021-01116-4
33. Alseekh S., Aharoni A., Brotman Y., et al. (2021). Mass spectrometry-based metabolomics: A guide for annotation, quantification and best reporting practices. *Nat. Methods* **18**:747–756. DOI:10.1038/s41592-021-01197-1
34. Johnson C. H., Ivanisevic J. and Siuzdak G. (2016). Metabolomics: Beyond biomarkers and towards mechanisms. *Nat. Rev. Mol. Cell Biol.* **17**:451–459. DOI:10.1038/nrm.2016.25
35. Naraoka H., Yamashita Y., Yamaguchi M., et al. (2017). Molecular evolution of N-containing cyclic compounds in the parent body of the Murchison meteorite. *ACS Earth Space Chem.* **1**:540–550. DOI:10.1021/acsearthspacechem.7b00058
36. Wolters C., Vuitton V., Orthous-Daunay F.-R., et al. (2023). Molecular screening with liquid chromatography coupled to utra-high-resolution Mass spectrometry: Chromatographic methods and data treatment for application to complex organic matter in astrophysical materials. *ACS Earth Space Chem.* **7**:1661–1674. DOI:10.1021/acsearthspacechem.3c00069
37. DiDonato N., Rivas-Ubach A., Kew W., et al. (2024). Improved characterization of soil organic matter by integrating FT-ICR MS, liquid xhromatography tandem Mass spectrometry, and molecular networking: A case study of root litter decay under drought conditions. *Anal. Chem.* **96**:11699–11706. DOI:10.1021/acs.analchem.4c00184
38. Pieczonka S. A., Thomas M. J., Schmitt-Kopplin P., et al. (2025). Harmonization of FT-ICR-MS instruments for interoperable multi-laboratory comprehensive compositional profiling. *Anal. Chem.* **97**:8491–8498. DOI:10.1021/acs.analchem.5c00488
39. Chan Q. H. S., Zolensky M. E., Kebukawa Y., et al. (2018). Organic matter in extraterrestrial water-bearing salt crystals. *Sci. Adv.* **4**:1–10. DOI:10.1126/sciadv.aao3521
40. Jones C. L. and Brearley A. J. (2006). Experimental aqueous alteration of the Allende meteorite under oxidizing conditions: Constraints on asteroidal alteration. *Geochim. Cosmochim. Acta* **70**:1040–1058. DOI:10.1016/j.gca.2005.10.029
41. Wang Y. and Hsu W. (2010). Petrology and mineralogy of the Ningqiang carbonaceous chondrite. *Meteorit. Planet. Sci.* **44**:763–780. DOI:10.1111/j.1945-5100.2009.tb00767.x
42. Rubin A. E., Trigo-Rodríguez J. M., Huber H., et al. (2007). Progressive aqueous alteration of CM carbonaceous chondrites. *Geochim. Cosmochim. Acta* **71**:2361–2382. DOI:10.1016/j.gca.2007.02.008
43. Lee M. R., Daly L., Floyd C., et al. (2021). CM carbonaceous chondrite falls and their terrestrial alteration. *Meteorit. Planet. Sci.* **56**:34–48. DOI:10.1111/maps.13607
44. Rudraswami N. G., Naik A. K., Tripathi R. P., et al. (2019). Chemical, isotopic and amino acid composition of Mukundpura CM2.0 (CM1) chondrite: Evidence of parent body aqueous alteration. *Geosci. Front.* **10**:495-504. DOI:10.1016/j.gsf.2018.02.001.
45. Schrader D. L., Davidson J., McCoy T. J., et al. (2021). The Fe/S ratio of pyrrhotite group sulfides in chondrites: An indicator of oxidation and implications for return samples from asteroids Ryugu and Bennu. *Geochim. Cosmochim. Acta* **303**:66–91. DOI:10.1016/j.gca.2021.03.019
46. Marrocchi Y., Avice G. and Barrat J.-A. (2021). The Tarda meteorite: A window into the formation of D-type asteroids. *Astrophys. J. Lett.* **913**:1–19. DOI:10.3847/2041-8213/abfaa3
47. Schrader D. L., Cloutis E. A., Applin D. M., et al. (2024). Tarda and Tagish lake: Samples from the same outer solar system asteroid and implications for D- and P-type asteroids. *Geochim. Cosmochim. Acta* **380**:48–70. DOI:10.1016/j.gca.2024.07.007
48. Lee M. R. and Nicholson K. (2009). Ca-carbonate in the Orgueil (CI) carbonaceous chondrite: Mineralogy, microstructure and implications for parent body history. *Earth Planet. Sci. Lett.* **280**:268–275. DOI:10.1016/j.epsl.2009.01.038
49. Gounelle M. and Zolensky M. E. (2014). The Orgueil meteorite: 150 years of history. *Meteorit. Planet. Sci.* **49**:1769–1794. DOI:10.1111/maps.12351
50. Jenkins L. E., Lee M. R., Daly L., et al. (2023). Winchcombe: An example of rapid

terrestrial alteration of a CM chondrite. *Meteorit. Planet. Sci.* **59**:988–1005. DOI:10.1111/maps.13949
51. Kebukawa Y., Mathurin J., Dartois E., et al. (2023). Complex mixture of organic matter in a xenolithic clast from the Zag meteorite revealed by coordinated analyses using AFM-IR, NanoSIMS and STXM/XANES. *Icarus* **400**:1–12. DOI:10.1016/j.icarus.2023.115582
52. Towers M. W., DeHoog R. J., Godfrey T. M., et al. (2026). Development of low-flow high-resolution desorption eectrospray ionization Mass spectrometry imaging. *J. Am. Soc. Mass Spectrom.* **37**:152–162. DOI:10.1021/jasms.5c00279
53. Johnson W. J., Palmer M. E., Claude E., et al. (2024). Combining enhanced resolving power with duty cycle limprovements on a multi-reflecting time-of-Flight Mass spectrometer. *J. Am. Soc. Mass Spectrom.* **35**:2073–2081. DOI:10.1021/jasms.4c00122
54. Liu H., Huang S., Yang L., et al. (2026). The application of desorption electrospray ionization mass spectrometry and mass spectrometry imaging in metabolomics, lipidomics and proteomics analysis. *Talanta* **297**:128611. DOI:10.1016/j.talanta.2025.128611
55. Pereira I., Ramalho R. R. F., Maciel L. I. L., et al. (2022). Directly mapping the spatial distribution of organic compounds on mineral rock surfaces by DESI and LAESI Mass spectrometry imaging. *Anal. Chem.* **94**:13691–13699. DOI:10.1021/acs.analchem.2c01154
56. Iqfath M., Wali S. N., Amer S., et al. (2024). Nanospray desorption electrospray ionization Mass spectrometry imaging (nano-DESI MSI): A Tutorial Review. *ACS Meas. Sci. Au* **4**:475–487. DOI:10.1021/acsmeasuresciau.4c00028
57. Guo J. and Huan T. (2020). Comparison of full-scan, data-dependent, and data-independent acquisition modes in liquid chromatography-Mass spectrometry based untargeted metabolomics. *Anal. Chem.* **92**:8072–8080. DOI:10.1021/acs.analchem.9b05135
58. Broeckling C. D., Beger R. D., Cheng L. L., et al. (2023). Current practices in LC-MS untargeted metabolomics: A scoping review on the use of pooled quality control samples. *Anal. Chem.* **95**:18645–18654. DOI:10.1021/acs.analchem.3c02924
59. Merel S. (2023). Critical assessment of the Kendrick mass defect analysis as an innovative approach to process high resolution mass spectrometry data for environmental applications. *Chemosphere* **313**:137443. DOI:10.1016/j.chemosphere.2022.137443
60. Wolf S., Schmidt S., Muller-Hannemann M., et al. (2010). In silico fragmentation for computer assisted identification of metabolite mass spectra. *BMC Bioinformatics* **11**:148. DOI:10.1186/1471-2105-11-148
61. Miller M. J., Kennedy A. D., Eckhart A. D., et al. (2015). Untargeted metabolomic analysis for the clinical screening of inborn errors of metabolism. *J. Inherit. Metab. Dis.* **38**:1029–1039. DOI:10.1007/s10545-015-9843-7
62. Garvie L. A. J., Trif L., Cotto-Figueroa D., et al. (2024). High surface area and interconnected nanoporosity of clay-rich astromaterials. *Sci. Rep.* **14**:1–11. DOI:10.1038/s41598-024-61114-2
63. Suttle M. D., King A. J., Schofield P. F., et al. (2021). The aqueous alteration of CM chondrites, a review. *Geochim. Cosmochim. Acta* **299**:219–256. DOI:10.1016/j.gca.2021.01.014
64. Milesi V., McCollom T. M. and Guyot F. (2016). Thermodynamic constraints on the formation of condensed carbon from serpentinization fluids. *Geochim. Cosmochim. Acta* **189**:391–403. DOI:10.1016/j.gca.2016.06.006
65. Kleber M., Bourg I. C., Coward E. K., et al. (2021). Dynamic interactions at the mineral–organic matter interface. *Nat. Rev. Earth Environ.* **2**:402–421. DOI:10.1038/s43017-021-00162-y
66. Erastova V., Degiacomi M. T., G. Fraser, D., et al. (2017). Mineral surface chemistry control for origin of prebiotic peptides. *Nat. Commun.* **8**:1–9. DOI:10.1038/s41467-017-02248-y
67. Viennet J. C., Roskosz M., Nakamura T., et al. (2023). Interaction between clay minerals and organics in asteroid Ryugu. *Geochem. Perspect. Lett.* **25**:8–12. DOI:10.7185/geochemlet.2307
68. Vinogradoff V., Le Guillou C., Bernard S., et al. (2020). Influence of phyllosilicates on the hydrothermal alteration of organic matter in asteroids: Experimental perspectives. *Geochim. Cosmochim. Acta* **269**:150–166. DOI:10.1016/j.gca.2019.10.029
69. He Y. Y., Bernard S., Lecasble M., et al. (2024). The evolution of amino acids under asteroidal aqueous alteration. *Geochim. Cosmochim. Acta* **387**:98–110. DOI:10.1016/j.gca.2024.09.035
70. Zanetta P. M., Le Guillou C., Leroux H., et al. (2022). Processes and temperatures of FGR formation in chondrites. *Geochim. Cosmochim. Acta* **319**:94–117. DOI:10.1016/j.gca.2021.11.019
71. Hanna R. D. and Ketcham R. A. (2018). Evidence for accretion of fine-grained rims in a turbulent nebula for CM Murchison. *Earth Planet. Sci. Lett.* **481**:201–211. DOI:10.1016/j.epsl.2017.10.029
72. Pinto G. A., Marrocchi Y., Jacquet E., et al. (2022). Formation of chondrule fine - grained rims from local nebular reservoirs. *Meteorit. Planet. Sci.* **57**:1004–1017. DOI:10.1111/maps.13812
73. Mouti Al - Hashimi X., Davidson J., Schrader D. L., et al. (2023). Fine - grained chondrule rims in Mighei - like carbonaceous chondrites: Evidence for a nebular origin and modification by impacts and recurrent solar radiation heating. *Meteorit. Planet. Sci.* **59**:789–808. DOI:10.1111/maps.14076
74. Zanetta P. M., Leroux H., Le Guillou C., et al. (2021). Nebular thermal processing of accretionary fine-grained rims in the Paris CM chondrite. *Geochim. Cosmochim. Acta* **295**:135–154. DOI:10.1016/j.gca.2020.12.015
75. Bland P. A. and Travis B. J. (2017). Giant convecting mud balls of the early solar system. *Sci. Adv.* **3**:1–10. DOI:10.1126/sciadv.1602514
76. Bland P. A., Jackson M. D., Coker R. F., et al. (2009). Why aqueous alteration in asteroids was isochemical: High porosity ≠ high permeability. *Earth Planet. Sci. Lett.* **287**:559–568. DOI:10.1016/j.epsl.2009.09.004
77. Muneishi K. and Naraoka H. (2021). Interactions between organic compounds and olivine under aqueous conditions: A potential role for organic distribution in carbonaceous chondrites. *Meteorit. Planet. Sci.* **56**:195–205. DOI:10.1111/maps.13614
78. Fujiya W., Sugiura N., Hotta H., et al. (2012). Evidence for the late formation of hydrous asteroids from young meteoritic carbonates. *Nat. Commun.* **3**:1–6. DOI:10.1038/ncomms1635
79. Yamaguchi A., Tomioka N., Ito M., et al. (2023). Insight into multi-step geological evolution of C-type asteroids from Ryugu particles. *Nat. Astron.* **7**:398–405. DOI:10.1038/s41550-023-01925-x
80. Tyra M. A., Farquhar J., Guan Y., et al. (2012). An oxygen isotope dichotomy in CM2 chondritic carbonates—A SIMS approach. *Geochim. Cosmochim. Acta* **77**:383–395. DOI:10.1016/j.gca.2011.10.003
81. Naraoka H., Hashiguchi M. and Okazaki R. (2022). Soluble Sulfur-Bearing Organic Compounds in Carbonaceous Meteorites: Implications for Chemical Evolution in Primitive Asteroids. *ACS Earth Space Chem.* **7**:41–48. DOI:10.1021/acsearthspacechem.2c00157
82. Zherebker A., Kostyukevich Y., Volkov D. S., et al. (2021). Speciation of organosulfur compounds in carbonaceous chondrites. *Sci. Rep.* **11**:1–13. DOI:10.1038/s41598-021-86576-6
83. Eberlin L. S., Ferreira C. R., Dill A. L., et al. (2011). Desorption electrospray ionization mass spectrometry for lipid characterization and biological tissue imaging. *Biochim. Biophys. Acta.* **1811**:946–960. DOI:10.1016/j.bbalip.2011.05.006
84. Lee M. R., Alexander C. M. O., Bischoff A., et al. (2025). Low-Temperature Aqueous Alteration of Chondrites. *Space. Sci. Rev.* **221**:1–59. DOI:10.1007/s11214-024-01132-8
85. Greenwood R. C., Franchi I. A., Findlay R., et al. (2022). Oxygen isotope evidence from Ryugu samples for early water delivery to Earth by CI chondrites. *Nat. Astron.* **7**:29–38. DOI:10.1038/s41550-022-01824-7
86. Sutton S., Alexander C. M. O. D., Bryant A., et al. (2017). The bulk valence state of Fe and the origin of water in chondrites. *Geochim. Cosmochim. Acta* **211**:115–132. DOI:10.1016/j.gca.2017.05.021
87. Tanaka R., Ratnayake D. M., Ota T., et al. (2024). Unraveling the Cr Isotopes of Ryugu: An Accurate Aqueous Alteration Age and the Least Thermally Processed Solar System Material. *Astrophys. J.* **965**:1–11. DOI:10.3847/1538-4357/ad276a
88. Shollenberger Q. R., Render J., Wimpenny J., et al. (2025). Elemental and isotopic signatures of Asteroid Ryugu support three early Solar System reservoirs. *Earth Planet. Sci. Lett.* **664**:1–8. DOI:10.1016/j.epsl.2025.119443
89. Yokoyama T., Wadhwa M., Iizuka T., et al. (2023). Water circulation in Ryugu asteroid affected the distribution of nucleosynthetic isotope anomalies in returned sample. *Sci. Adv.* **9**:1–11. DOI:10.1126/sciadv.adi7048
90. Potiszil C., Ota T., Yamanaka M., et al. (2025). Meteoritic and asteroidal amino acid heterogeneity: Implications for planetesimal alteration conditions and sample return missions. *Earth Planet. Sci. Lett.* **653**:1–12. DOI:10.1016/j.epsl.2025.119205
91. Naraoka H. and Hashiguchi M. (2019). Distinct distribution of soluble N-heterocyclic compounds between CM and CR chondrites. *Geochem. J.* **53**:33–40. DOI:10.2343/geochemj.2.0546
92. Li Y., Kurokawa H., Sekine Y., et al. (2023). Aqueous breakdown of aspartate and glutamate to n-omega-amino acids on the parent bodies of carbonaceous chondrites and asteroid Ryugu. *Sci. Adv.* **9**:1–15. DOI:10.1126/sciadv.adh7845
93. Amano K., Viennet J.-C., Beck P., et al. (2025). Updating the Urey-Craig diagram: The iron redox states of the building blocks of the outer solar system. *Earth Planet. Sci. Lett.* **669**:1–13. DOI:10.1016/j.epsl.2025.119587
94. Choi B.-G. and Wasson J. T. (2003). Microscale oxygen isotopic exchange and magnetite formation in the Ningqiang anomalous carbonaceous chondrite. *Geochim. Cosmochim. Acta* **67**:4655–4660. DOI:10.1016/s0016-7037(03)00390-9
95. DeMeo F. E. and Carry B. (2014). Solar system evolution from compositional mapping of the asteroid belt. *Nature* **505**:629–634. DOI:10.1038/nature12908
96. Fujiya W., Hoppe P., Ushikubo T., et al. (2019). Migration of D-type asteroids from the outer solar system inferred from carbonate in meteorites. *Nat. Astron.* **3**:910–915. DOI:10.1038/s41550-019-0801-4
97. DeMeo F. E., Binzel R. P., Slivan S. M., et al. (2009). An extension of the Bus asteroid taxonomy into the near-infrared. *Icarus* **202**:160–180. DOI:10.1016/j.icarus.2009.02.

005
98. Vilas F. and Smith B. A. (1985). Reflectance spectrophotometry (~0.5–1.0 μm) of outer-belt asteroids: Implications for primitive, organic solar system material. *Icarus* **64**:503-516. DOI:10.1016/0019-1035(85)90071-5
99. Mimura K., Okumura F. and Harada N. (2020). Constraints on the thermal history of the Allende (CV3) meteorite by gradual and stepwise pyrolyses of insoluble organic matter. *Geochem. J.* **54**:255–265. DOI:10.2343/geochemj.2.0589
100. Cronin J. R. and Moore C. B. (1971). Amino Acid analyses of the murchison, murray, and allende carbonaceous chondrites. *Science* **172**:1327–1329. DOI:10.1126/science.172.3990.1327
101. Nakamura T., Matsumoto M., Amano K., et al. (2023). Formation and evolution of carbonaceous asteroid Ryugu: Direct evidence from returned samples. *Science* **379**:1–15. DOI:10.1126/science.abn8671
102. Furukawa Y., Saigusa D., Kano K., et al. (2023). Distributions of CHN compounds in meteorites record organic syntheses in the early solar system. *Sci. Rep.* **13**:1–12. DOI:10.1038/s41598-023-33595-0
103. McCollom T. M. (2013). The influence of minerals on decomposition of the n-alkyl-α-amino acid norvaline under hydrothermal conditions. *Geochim. Cosmochim. Acta* **104**:330–357. DOI:10.1016/j.gca.2012.11.008
104. He Y., Rémusat L., Lecasble M., et al. (2024). Evolution of Nucleobases under asteroidal aqueous alteration. *ACS Earth Space Chem.* **8**:1820–1831. DOI:10.1021/acsearthspacechem.4c00132
105. Fujiya W., Kawasaki N., Nagashima K., et al. (2023). Carbonate record of temporal change in oxygen fugacity and gaseous species in asteroid Ryugu. *Nat. Geosci.* **16**:675–682. DOI:10.1038/s41561-023-01226-y
106. Munoz Caro G. M., Carrascosa de Lucas H. and Martin-Domenech R. (2025). Photochemistry of interstellar ice forming complex organic molecules. *Nat. Rev. Chem.* **9**:537–552. DOI:10.1038/s41570-025-00729-z
107. Bose M., Root R. A. and Pizzarello S. (2017). A XANES and Raman investigation of sulfur speciation and structural order in Murchison and Allende meteorites. *Meteorit. Planet. Sci.* **52**:546–559. DOI:10.1111/maps.12811
108. Yabuta H., Williams L. B., Cody G. D., et al. (2010). The insoluble carbonaceous material of CM chondrites: A possible source of discrete organic compounds under hydrothermal conditions. *Meteorit. Planet. Sci.* **42**:37–48. DOI:10.1111/j.1945-5100.2007.tb00216.x
109. Isa J., Orthous-Daunay F.-r., Beck P., et al. (2021). Aqueous alteration on asteroids simplifies soluble organic matter mixtures. *Astrophys. J. Lett.* **920**:1–14. DOI:10.3847/2041-8213/ac2b34
110. Chan Q. H. S., Nakato A., Kebukawa Y., et al. (2018). Heating experiments of the Tagish lake meteorite: Investigation of the effects of short - term heating on chondritic organics. *Meteorit. Planet. Sci.* **54**:104–125. DOI:10.1111/maps.13193
111. Danger G., Ruf A., Javelle T., et al. (2022). The transition from soluble to insoluble organic matter in interstellar ice analogs and meteorites. *Astron. Astrophys.* **667**:1–15. DOI:10.1051/0004-6361/202244191
112. Kipfer K. A., Ligterink N. F. W., Riebe M. E. I., et al. (2025). The formation of organic macromolecular matter from the electron irradiation of simple carbon-containing ices. *Astron. Astrophys.* **702**:1–12. DOI:10.1051/0004-6361/202555840
113. Schuepfer D. B., Badaczewski F., Guerra-Castro J. M., et al. (2020). Assessing the structural properties of graphitic and non-graphitic carbons by Raman spectroscopy. *Carbon* **161**:359–372. DOI:10.1016/j.carbon.2019.12.094

FUNDING AND ACKNOWLEDGMENTS

National Natural Science Foundation of China (62227901, 42425303, 42241103), Key Research Program of the Institute of Geology and Geophysics, Chinese Academy of Sciences (IGGCAS-202101, IGGCAS-202401) We especially acknowledge the Waters Corporation for providing instrument sponsor and technique support. We thank Xiaofei Jia (Waters), Wei Zheng (Waters), Weiwei Dong (Waters), Jianlan Yu (Waters), Qing Li (Waters), Yuyang He, and Chi Zhang for assistance in the experiments, and Ross N. Mitchell, Sanzhong Luo, Yu Xia for constructive discussions. The funders had no role in study design, data collection and analysis, decision to publish, or preparation of the manuscript.

AUTHOR CONTRIBUTIONS

Conceptualization: Mingtan Dong, Wei Yang. Methodology: Mingtan Dong, Wei Yang, Jialong Hao. Investigation: Mingtan Dong. Visualization: Mingtan Dong, Wei Yang. Funding acquisition, Project administration and Supervision: Wei Yang. Writing – original draft: Mingtan Dong, Wei Yang. Writing – review & editing: Jialong Hao, Sen Hu, Yangting Lin. All authors contributed to the manuscript and approved the final version.

DECLARATION OF INTERESTS

Wei Yang is an Editorial Board member of The Innovation Geoscience and was blinded from reviewing or making final decisions on the manuscript. Peer review was handled independently of this member and their research group. The other authors declare no conflicts of interest.

DATA AND CODE AVAILABILITY

Raw data for review and further processing are available from the corresponding author upon reasonable request, either via remote access or as a hard-drive copy.

SUPPLEMENTAL INFORMATION

It can be found online at https://doi.org/10.59717/j.xinn-geo.2026.100199